Biophysical Chemistry 302 (2023) 107098

Contents lists available at ScienceDirect

Biophysical Chemistry

journal homepage: www.elsevier.com/locate/biophyschem

Asymmetrical interactions between nanoparticles and proteins arising from deformation upon adsorption to surfaces

Megan Maniar, Joachim Kohn, N. Sanjeeva Murthy *

Laboratory for Biomaterials Research, Department of Chemistry and Chemical Biology, Rutgers University, Piscataway, NJ 08854, USA

ARTICLE INFO

Keywords:
Nanoparticles
Protein adsorption
Immobilization
Interactions
Quartz crystal microbalance
XPS
SAXS

ABSTRACT

Drug release from polymeric nanoparticles (NPs) is governed by their adsorption onto cell membranes and transmigration across cell walls. These steps are influenced by their interactions with proteins near the cells. These interactions were investigated by studying the sequential adsorption of plasma proteins, albumin (Alb) and fibrinogen (Fg), and micellar NPs using quartz crystal microbalance with dissipation (QCMD), X-ray photoelectron spectroscopy (XPS), and small-angle X-ray scattering (SAXS). The three NPs in the study all have poly (ethylene glycol) (PEG) shells but different cores: amorphous poly(propylene oxide) (PPO), crystalline polycaprolactone (PCL), and poly(desaminotyrosyl-tyrosine octyl ester-*co*-suberic acid) (DTO-SA). None of the NPs adsorbed onto a pre-adsorbed Fg layer. On the other hand, when the deposition sequence was reversed, Fg was adsorbed onto DTO-SA NP and PCL NP surfaces, but not onto the PPO NP surface. The interactions with Alb were different: DTO-SA did not adsorb onto Alb and vice versa; PPO NP adsorbed onto an Alb layer, but Alb did not adsorb onto the PPO NP layer; and PCL NP reversibly adsorbed onto Alb, but Alb displaced pre-adsorbed PCL NP. Thus, in most instances, the adsorption behavior was asymmetric in that it was dependent on the order of arrival of the adsorbates at the substrate. SAXS data did not show evidence for complex formation in solution. Thus, the solution behavior appears not to be a predictor of the interaction of proteins and the NPs near surfaces. Differing strengths of pairwise interactions of proteins, NPs and substrates account for this adsorption behavior. These differences in interactions could be the results of deformation of the adsorbates immobilized at the surface and the different degrees of surface remodeling that occur upon adsorption. Deformation could lead to disassembly of the NPs that has implications on their ability to release their payload of drugs upon adsorption onto tissue surfaces.

1. Introduction

Polymeric nanoparticles (NPs) are widely used in many health care applications as nanocarriers for gene delivery, targeted and controlled release of drugs, vaccination, cancer treatments, and imaging [1–3]. They are also incorporated into implanted scaffolds to engineer and regenerate tissue [4,5]. These NPs, made from amphiphilic molecules, are ideal carriers for drug molecules since their hydrophobic core interacts favorably with drugs, many of which are hydrophobic, while the hydrophilic shell solubilizes the drug-carrying NPs in aqueous media. Successful application of NPs in biomedical application requires a careful design of their composition of the NPs to modulate the protein corona around them. In turn, this protein corona affects the NPs transport through biological milieu, adsorption onto cells and subsequent disassembly for eventual drug release at the target site [6]. These issues have been addressed by a detailed investigation of the understanding of the interactions between NPs and proteins [7–10], and with biological substrates in general [11–13]. Despite the recent success of NPs in these applications, such as the use of lipid NPs delivering mRNA vaccines, their full potential has not yet been fully realized, especially with polymeric NPs [14].

Polymeric NPs are formed by self-assembly of amphiphilic block copolymer chains [9,15], either A-B diblock or A-B-A triblock copolymers, where A is the hydrophilic component and B is the hydrophobic component. These chains form micelles in aqueous media as hydrophobic blocks aggregate to form an inner core surrounded by an outer shell of hydrophilic segments. To study the influence of NP's core-shell structure on their interactions with proteins, we investigate here three types of NPs in which methoxy poly(ethylene glycol) or PEG, is the hydrophilic component (A-block), as is the case in majority of polymeric

* Corresponding author.
E-mail address: murthy@chem.rutgers.edu (N.S. Murthy).

https://doi.org/10.1016/j.bpc.2023.107098
Received 6 June 2023; Received in revised form 9 August 2023; Accepted 21 August 2023
Available online 23 August 2023

NPs. The three NPs differ in their hydrophobic B-blocks, which are desaminotyrosyl-tyrosine octyl ester, poly(propylene oxide), and poly (ε-caprolactone), identified as DTO-SA NP, PPO NP, and PCL NP, respectively. The PPO-based triblock copolymers are commercially available as Pluronics® (BASF) and are also known as Poloxamers.

One reason that NPs have not met expectations as efficient drug delivery devices is because their interactions with the plasma proteins as they are transported to cells, and with cell membranes prior to drug release, is more complex than is currently understood. Current models rarely consider the influence of deformation of NPs and plasma proteins upon adsorption onto surfaces on their mutual interactions, and their subsequent interactions with the constituents of the cell membranes [16]. Furthermore, little is known about the role played by the structure of the NPs, specifically the core-shell morphology of the NPs, on drug release. We address these issues, and also explore the possibility of the extension of the Vroman effect, which was originally postulated in the context of plasma proteins, to other particles, in this instance to NPs. We use quartz crystal microbalance with dissipation (QCMD) to monitor the adsorption behaviors of NPs to proteins to a substrate that serves as a proxy for cell membranes, and their mutual interactions when one of the species is adsorbed. Small-angle X-ray scattering (SAXS) was used to study the inter-particle interactions in solution. X-ray photoelectron spectroscopy (XPS) data were obtained to validate the QCMD results.

2. Materials and methods

2.1. Preparation and characterization of NPs

The NPs used in this report (Fig. 1) are described in our previous publications, and the references cited therein [17,18]. Briefly, the first NP used in this study is from a triblock copolymer, PEG-*block*-oligo-(desaminotyrosyl-tyrosine octyl ester suberate)-*block*-PEG, abbreviated as DTO-SA. The number-average molecular weight (M_n) of PEG is 5 kDa and that of the middle block is 14 kDa. The second NP is from Pluronic F-127 (Sigma Aldrich, also known as Poloxomer 407) and is identified as PPO NP; the molecular weight of the central PPO block is 3.8 kDa, and that of the end blocks PEO are 4.4 kDa. The third NP is from PEG-*block*-PCL, identified as PCL NP (Sigma-Aldrich; Product# 570303 - 250 mg); the molecular weights of PEG and PCL blocks were 5 kDa. All three NPs were characterized by dynamic light scattering (DLS) using a particle size analyzer (Malvern, Zetasizer Nano-S) [18].

2.2. Protein solutions

Albumin (Alb) and fibrinogen (Fg) were purchased from Sigma-aldrich (Alb: Bovine serum albumin, A4503-10G, Lot # SLBT8839, cold ethanol fraction, pH 5.2, ≥ 96%; Fg: Bovine fibrinogen, F8620-1G Lot # 021M7352V). 5 mg/ mL solutions of the two proteins were prepared in phosphate buffered saline (pH 7.0) (PBS) (Sigma-Aldrich Dulbecco's, D8537-500 μL, Lot # RNBGO544, modified, without calcium chloride and magnesium chloride, liquid, sterile-filtered). 5 mg/ mL concentration was found to give complete surface coverage as seen by the plateau in adsorbed mass (frequency change in QCMD) vs. concentration plots (Fig. S1).

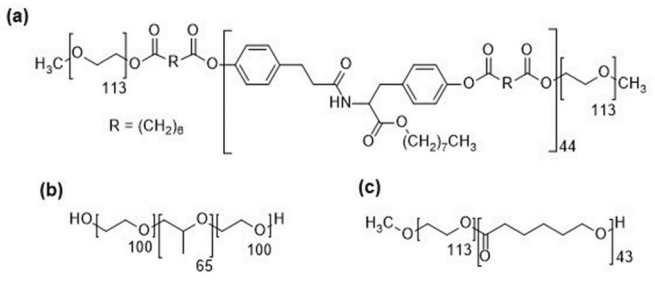

Fig. 1. (a) Structures of the copolymers used to fabricate the NPs. (a) Tyrosine-derived copolymer. (b) Pluronic F-127. (c) PEG−PCL.

2.3. Preparation of the substrates

The adsorption measurements were carried out on polymer-coated gold QCMD sensors (Biolin Scientific, Gothenburg, Sweden). A hydrophobic polymer made of desaminotyrosyl-tyrosine ethyl ester with carbonate linkages, identified as E0000 (E for ethyl ester and 0000 for the absence of any comonomers), was deposited on to the sensors by spin coating [19,20]. E0000 was chosen instead of a common polymer such as polystyrene because it is a member of a family of polymers being developed in our laboratory for fabricating scaffolds for tissue engineering [21–25]. Such a polymer coating eliminates the ambiguities in adsorption arising from the roughness of the gold surface [26].

2.4. Adsorption experiments

Protein and NPs were deposited onto the QCMD sensors by flowing the respective solutions over the substrate. The depositions were done sequentially. NP (1 mg/mL) and protein solutions (5 mg/mL) were passed over the sensors in the desired sequence at a flow rate of 20 μl/min. The protein solutions were allowed to flow for 20 min and the polymer solutions for 10 min. The sensor was rinsed for 5 min with PBS before and after the run. Our previous work using XPS and atomic-force microscopy has shown that NPs completely cover the hydrophobic substrate deposited on gold [18]. This work also demonstrated that once the three NPs, Alb, and Fg are adsorbed onto E0000, they do not rinse off. Therefore, no rinsing step was included after each individual adsorption step.

2.5. Quartz crystal microbalance with dissipation (QCMD)

Frequency (f) and dissipation (D) data were collected on a Q-Sense Omega instrument (Biolin Scientific) at 37 °C. Gold-coated sensors were purchased from Nanoscience Instruments (Phoenix, AZ). An average of six measurements was made for each experimental condition, with a minimum of three and sometimes as many as many as twelve. Data were analyzed using the QTools software supplied by the instrument manufacturer.

QCMD data are typically presented as the changes in the frequency of oscillation of the quartz sensor crystal (Δf), and the changes in dissipation (ΔD) [27–29]. If ΔD is small, then Δf can be used determine the adsorbed mass (Δm). A decrease in frequency indicates adsorption and conversely an increase in frequency indicates mass loss, as given by the Sauerbrey equation: $\Delta m = -(C/n)\Delta f$, where C is the mass sensitivity constant (17.7 ng/cm^2), and n is the overtone number (1, 3, …) [28]. ΔDs were small in many instances, but in some instances, they were between 0.8 and 1.6 × 10^{-6} units per 10 Hz in Δf, which are a little higher than the threshold (0.5 × 10^{-6} units per 10 Hz) for using the Sauerbrey equation. When ΔDs, which reflect the viscoelastic properties of the adsorbed layers, are large Sauerbrey equation does not hold. In these instances, the Voigt model was used to analyze the data to obtain the adsorbed thickness assuming a density of 1150 Kg/cm^3, and the shear modulus of the adsorbed layers [28].

2.6. X-ray photoelectron spectroscopy (XPS)

Chemical analysis of the surfaces after the QCMD experiments was carried out on a K-Alpha XPS (Thermo Fisher Scientific, Waltham, MA). A 1486 eV electron beam (0.4 mm diameter) from an Al Kα source was used to collect C 1 s, N 1 s, and O 1 s core-level spectra (10 scans, dwell time of 50 ms, and a pass energy of 50 eV). The spectra were analyzed using the Avantage XPS software available on the instrument. Six peaks were fitted for the carbon core-level: C − C (285.0 eV), C − O (286.6 eV), amide (288.0 eV), ester/carboxyl (289.1 eV), carbonate (290.8 eV), and

π − π satellite (291.8 eV) [30]. Peaks with 70% Gaussian, 30% Lorentzian, and a full-width at half-maxima (FWHM) <2 eV were used. O core-level peak widths were fixed to be the same as those of the O═C peaks. Details of the analysis are given in a previous publication [18].

2.7. Small-angle X-ray scattering (SAXS)

Solution scattering data were collected at the Life Science X-ray scattering (LIX) beam line (16ID), National Synchrotron Light Source II (NSLS-II), Brookhaven National Lab (Upton, NY). Data were collected over a q range of 0.005–3.040 $Å^{-1}$ (0.005–0.25 $Å^{-1}$ data used for this report) with a wavelength of 0.8172 Å (15.170 keV). Polymer concentration was 1 mg/mL and exposure times were 5 s. The counts from five exposures were averaged and appropriate background subtracted for further analysis. Guinier, Porod, and pair distribution function plots were obtained using BioXtas software [31].

3. Results

3.1. QCMD adsorption of NPs and proteins

The Δf-ΔD data obtained during the sequential adsorption of the NPs onto protein layers, and of proteins onto the NP layers, are shown in Fig. 2. The results are tabulated in Table 1. The first two columns in Fig. 2 are from experiments with Alb, and the second two are with Fg. In each pair, the first column shows the adsorption data that begins with a protein and is followed by a NP. The frequency shifts by ~20 Hz after Alb adsorption and by ~90 Hz after Fg; these are in agreement with the values reported in the literature [32,33]. The second column in each pair shows the data that begins with the adsorption of NPs followed by a protein. Adsorption of NPs causes the frequency to decrease by approximately 50, 40, and 30 Hz with DTO-SA-, PPO- and PCL-based NPs, respectively. This compares favorably with the previously reported values [18]. The data in Fig. 2 are described below. The observations are illustrated in Fig. 3.

3.1.1. Sequential deposition with Alb

There is no significant change in frequency when the adsorption of Alb is followed by DTO-SA NP (Fig. 2a), indicating that these NPs do not bind to the pre-adsorbed Alb layer. Similar non-adsorptive behavior is seen when the sequence is reversed (Fig. 2b). In contrast, PPO NP adsorbs onto Alb as shown by the large drop in frequency with only a small change upon subsequent rinsing (Fig. 2e), indicating irreversible adsorption (also see XPS data, Fig. 4b). When the sequence is reversed, the frequency remains essentially unchanged when Alb flows over PPO NP (a small increase suggests in fact some mass loss) indicating that Alb does not adsorb onto NP (Fig. 2f). Thus, the PPO NP-Alb interaction is asymmetric. PCL NPs also adsorb onto Alb, but this is reversible as indicated by the NPs being removed upon rising with buffer; this can be seen by the return of many of the Δf and ΔD harmonics back to pre-PCL NP values (Fig. 2i, two out of three in the figure). This reversible adsorption is confirmed by XPS data (Fig. 4b). When the sequence is reversed, there is a large increase in frequency after the adsortion of Alb onto NPs (Fig. 2j). Based on XPS data presented in section 3.2, we attribute this increase in frequency to the displacement of the PCL NPs by Alb.

3.1.2. Sequential deposition with Fg

Absence of any significant frequency shift upon injection of NPs following Fg (Figs. 2c, g, and k) indicates that none of the NPs are adsorbed onto the pre-adsorbed Fg layer; small changes in frequency suggest some surface remodeling, including co-location. The interaction

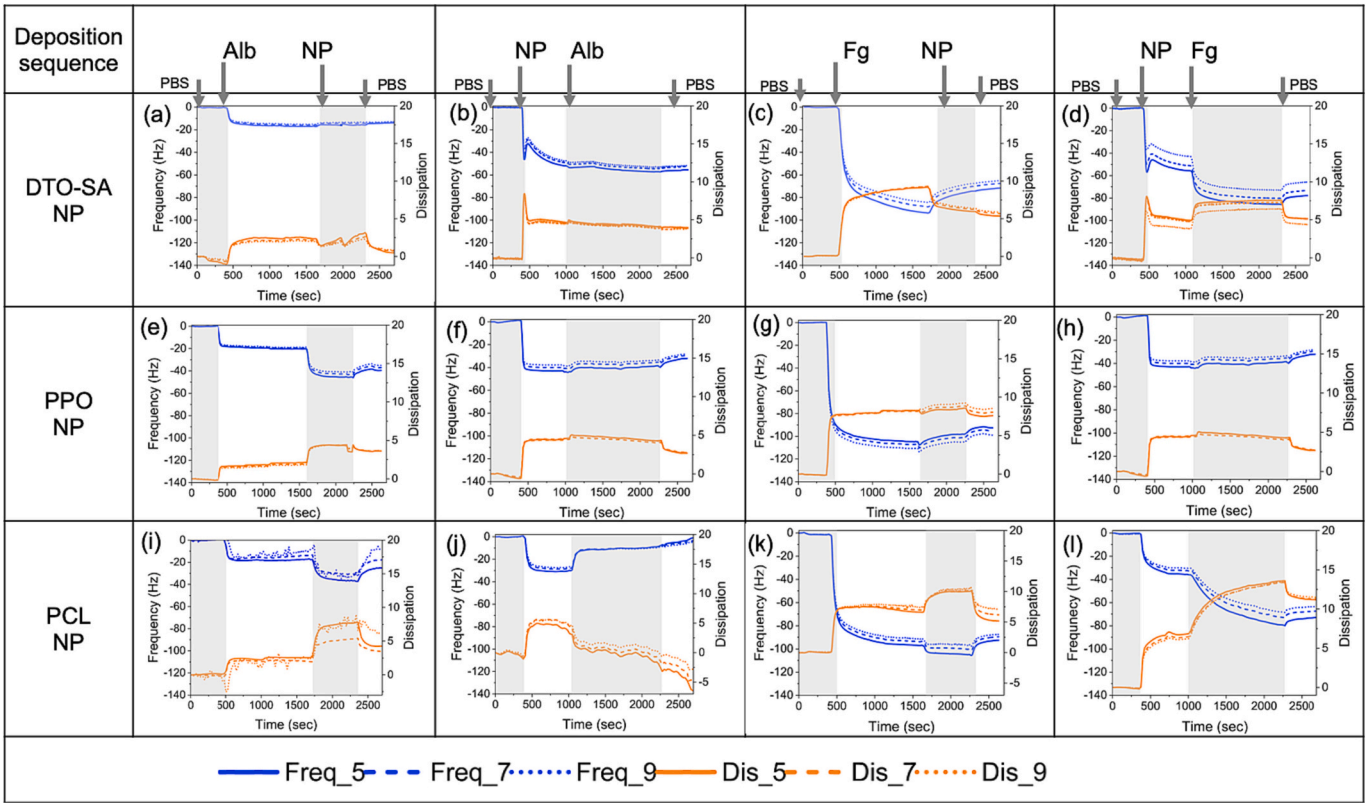

Fig. 2. QCMD data in the form of frequency and dissipation versus time curves for the sequential adsorption of the two proteins and the three NPs, as indicated in the column headings. In each panel, the top curves (blue) are frequency responses, and the bottom curves (red) are the corresponding dissipation changes for overtone 5, 7, and 9. In each panel, the sensor is equilibrated with PBS for the first 500 s. Next, the first adsorbate is injected. This is followed by the second adsorbate. Finally, the sensor is rinsed with PBS. (For interpretation of the references to colour in this figure legend, the reader is referred to the web version of this article.)

Table 1
Changes in the frequencies (5th harmonic, in Hz) corresponding to Fig. 2 in the main text. Standard deviations are shown in parenthesis. There are four pairs of data in eight columns corresponding to the columns in Fig. 3.

Deposition sequence	Alb	NP	NP	Alb	Fg	NP	NP	Fg
				DTO-SA				
Δf (Hz)	−14.3	+1.3	−48.7	−1.5	−83.0	+10.6	−46.3	−37.3
	(1.9)	(0.8)	(7.5)	(3.4)	(9.9)	(5.9)	(7.5)	(12.7)
Voigt Thickness (nm)	4.2	3.2	24	24	41	36	37	36
G (kPa)	200	205	6.5	5	27	12	14	12
				PPO				
Δf (Hz)	−19.9	−24.2	−44.3	+2.3	−122.4	+6.3	−42.7	+5.1
	(1.4)	(6.1)	(2.3)	(0.6)	(7.4)	(3.1)	(9.8)	(4.0)
Voigt Thickness (nm)	4	8.5	8	7.5	28	32	4.7	3.8
G (kPa)	280	460	420	380	50	22	500	420
				PCL				
Δf (Hz)	−13.7	−19.8	−33.7	+22.9	−103.3	−10.0	−32.5	−48.5
	(3.1)	(3.9)	(4.6)	(9.9)	(16.3)	(6.3)	(9.8)	(8.3)
Voigt Thickness (nm)	4	12	8.5	4	35	42	13.8	20
G (kPa)	190	80	240	412	37	30	109	220

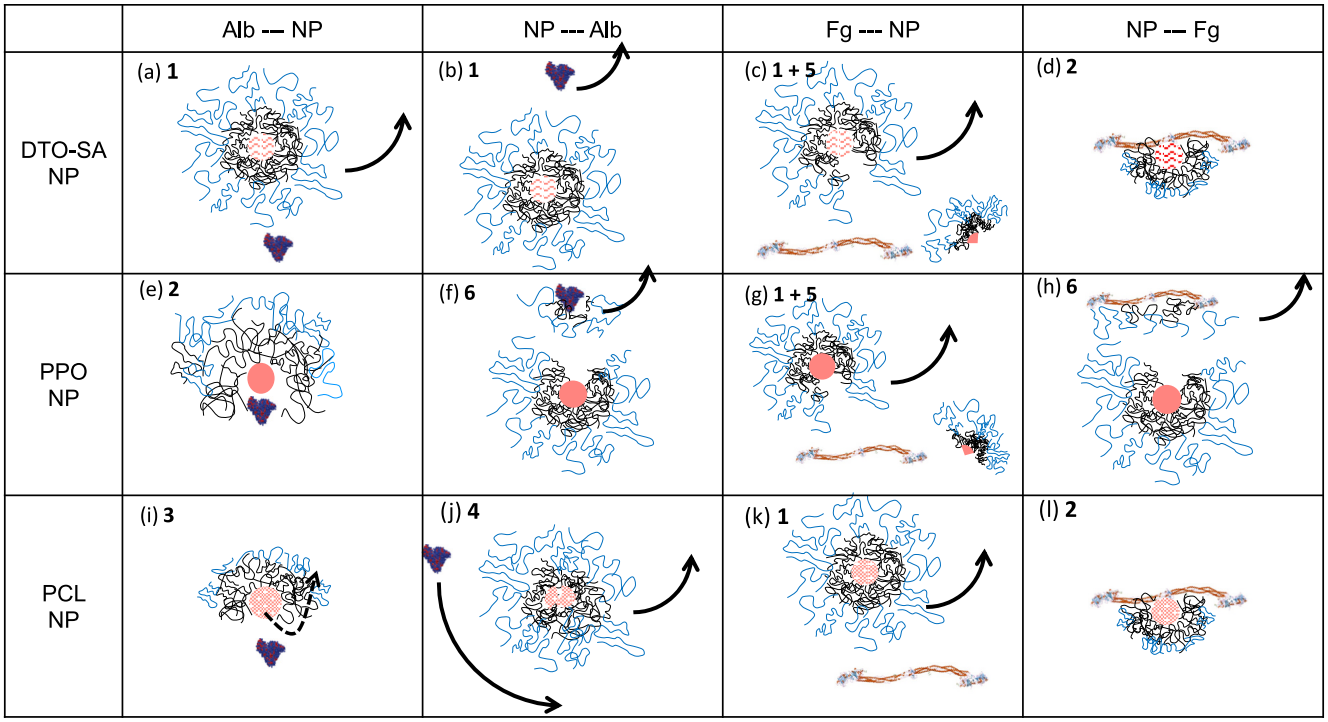

Fig. 3. Schematics illustrate the proposed modes of interactions between the NPs and the proteins based on the QCMD data. NPs and proteins are depicted to scale. Deposition sequence is shown in the column headings, and the three rows correspond to the three NPs. Numbers 1–6 next to the figure labels identify the different mechanisms: 1-No adsorption. 2-Irreversible adsorption. 3-Reversible adsorption. 4-Displacement. 5-Colocation. 6-Ablation.

of Fg with the pre-adsorbed NP layer depends on the NP. Decrease in frequency with DTO-SA NP and PCL NP (Figs. 2d and l), and a large increase in the nitrogen signal in XPS (see section 3.2), indicate that Fg is being adsorbed onto DTO-SA and PCL NPs. This interaction is asymmetric since these NPs do not, or only weakly, adsorb onto the pre-adsorbed Fg layer (Figs. 2c and k). A small increase in frequency with PPO NP followed by Fg (Fig. 2h) indicates mass loss or remodeling of the surface as in the case with Fg followed by PPO NP; the interaction is symmetric.

3.1.2.1. Voigt analysis of the data. The data were analyzed using the Voigt model to obtain the thickness corrected for dissipation and the shear moduli (G) of the adsorbed layers. The results (Table 1) are from one representative scan of each of the samples that was analyzed with different combinations of harmonics 2–6. We found that there are large uncertainties in the G values derived from Voigt fitting, and therefore we will use these values for qualitative comparisons only.

Shear moduli of 200–300 kPa for Alb and 20–50 kPa for Fg are consistent with the reported values for these two proteins [33,34]. The higher modulus calculated for Alb relative to Fg validates the use of the Voigt model for data analysis. The moduli of the three NPs are ~10, 500, and 200 for DTO-SA, PPO, and PCL NPs, respectively. These differences are indicative of the core-shell interactions and the deployment of the shell PEG segments into the surrounding aqueous medium.

Upon adsorption of NP onto the pre-adsorbed Alb layer, the modulus remains unchanged with DTO-SA NP, increases with PPO NP, and decreases with PCL NP, consistent with the illustration in Figs. 3a, e, and i, respectively. When the sequence is reversed, the modulus is unchanged with DTO-SA and PPO NPs, but increases with PCL NP, reflecting significant interactions between PCL NP and Alb.

Upon adsorption of NP onto a pre-adsorbed Fg layer, the change in the modulus is small, indicating the absence of any significant Fg-NP

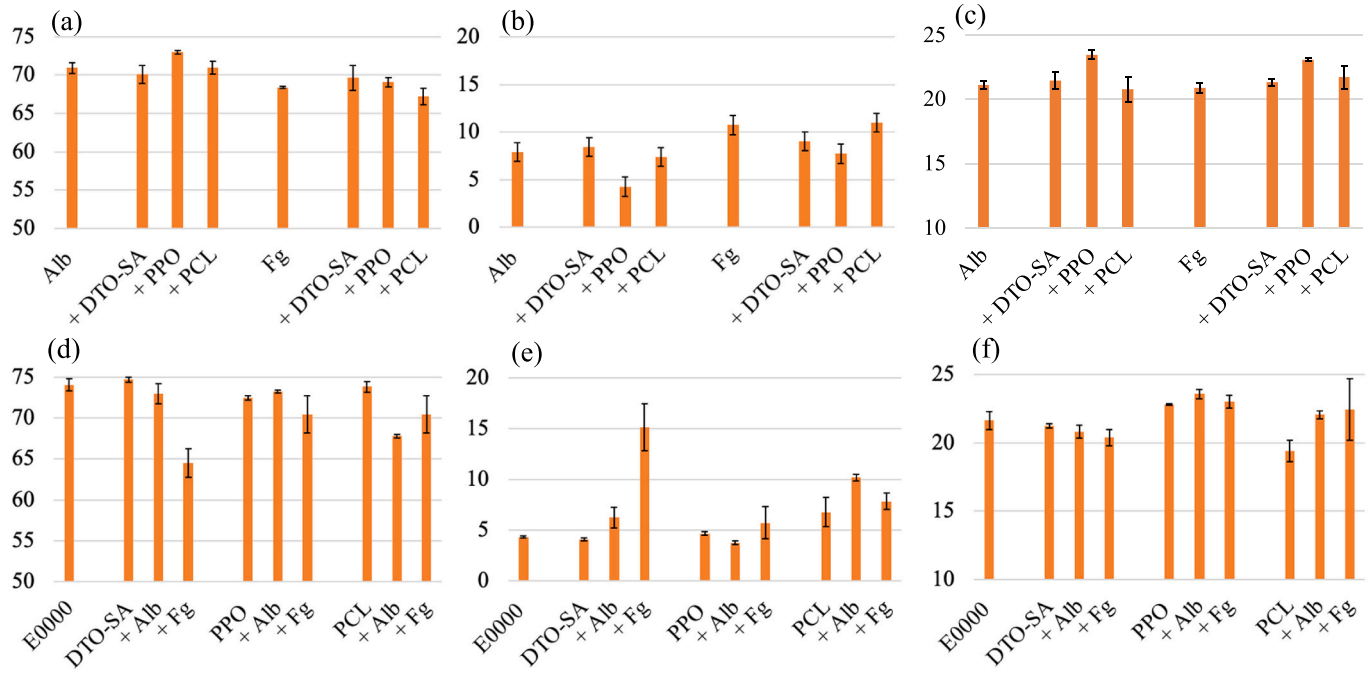

Fig. 4. Top row: Protein followed by NP. (a) C1s. (b) N1s. (c) O1s. Bottom row: NP followed by protein. (d) C1s. (e) N1s. (f) O1s.

interactions; a small decrease with all three NPs, suggests remodeling of the adsorbed Fg layer by some NP fragments. This is also suggested by small changes in the thickness. The surface remodeling explains the decrease in N signals with DTO-SA and PPO NPs. When the sequence is reversed, the modulus remains unchanged with DTO-SA NP, decreases with PPO NP, and increases with PCL NP, indicating different degrees of binding between the pre-adsorbed NPs and the incoming Fg.

3.2. XPS

The surface elemental composition of the layers deposited on the QCMD sensors during the experiment was determined using XPS. Because of the presence of amino acids in the proteins, increase in N content or decrease in C content relative to the control (E000) indicates the presence of protein at the surface. Conversely, lower N and higher C contents relative to the control indicates segments of the NP at the surface. Ultrahigh vacuum environment in the XPS chamber can change the surface structure from that in the aqueous medium in the QCMD module by causing the NPs and protein to deform and fragment, and otherwise rearrange. However, nitrogen and oxygen concentrations will not be affected by the surface rearrangement since it is unlikely that the molecules in the dry sample will mix in the z-direction, a processs that can be facilated by the aqueous medium during the QCMD measurements. We have established that there is complete coverage of the gold by E0000 polymers. We have also ensured that there is complete coverage of the surface by the NPs and the proteins by using the appropriate concentrations, 1 and 5 mg/mL, respectively\. Thus, we can use the XPS data to validate the observations based in QCMD data. The results shown in Fig. 4 were obtained from detailed profile analyses of the XPS scan as described in an earlier publication [18]. Examples of the survey scans on six representative surface are shown in Fig. S3. These results are consistent with the scheme shown in Fig. 3 derived from the QCMD data as discussed below.

If we examine the deposition of the NPs onto a pre-adsorbed Alb layer (Figs. 4a, b, and c), we see that C and N values do not change significantly with DTO-SA and PCL NPs. This is consistent with the non-adsorption of DTO-SA NP onto Alb (Fig. 2a), and the reversible adsorption of PCL NP onto Alb (Fig. 2i) deduced based on QCMD data. There is noticeable increase in C and a large decrease in N with PPO NP. This shows that PPO NP is the topmost layer and this adsorption of PPO NP onto the Alb layer is consistent with the QCMD results (Fig. 2e).

In the deposition of the NPs onto a pre-adsorbed Fg layer, in contrast, we see marginal changes in the composition at the surface (Figs. 4a, b, and c). There is a small increase in C and a small decrease in N with DTO-SA NP, a larger decrease with PPO NP, and no change with PCL NP. This suggests with DTO-SA and PPO NPs, fragments of NP might be covering the Fg surface or co-located with Fg, and very little interaction between PCL NP and Fg. For the most part there is no adsorption of Fg as deduced from the QCMD data (Figs. 2b, f, and j).

We now examine the adsorption behavior when the sequence is reversed such that protein is adsorbed onto the pre-adsorbed NP layer (Figs. 4d, e, and f). With Alb, we see little change in either C or N content at the surface DTO-SA and PPO NPs, indicating that Alb does not interact with these adsorbed NPs. However, with PCL NPs, we see that C decreases and N increases. This, combined with the QCMD data (Fig. 2j), suggests that Alb displaces PCL NPs. With Fg, there is a large decrease in C and an increase in N when DTO-SA NPs are adsorbed onto the surface first. There are similar, but smaller, changes with PCL NP. This suggests that Fg is adsorbed on top of the DTO-SA and PCL NPs. In contrast, very little change in both the C and N content with PPO NPs shows little interaction of Fg with this NP.

3.3. SAXS

SAXS data are presented in Fig. 5 in the form of pair distribution functions, $P(r)$, which represent the shape and the size of the particle [35]. The $P(r)$ functions for the two proteins are similar to that reported in the literature, extending to <100 Å for Alb [36], and >500 Å for Fg [37]. The $P(r)$ functions suggest DTO-SA NP to be a compact globular particle, PPO NP to be a disc, and PCL NP to be a cylinder [35]. These differences are expected in micellar structures and are determined by the distribution of the hydrophobic segments in the core and PEG chains in the shell [35]. The $P(r)$ functions of the mixtures can be interpreted as a superposition of the $P(r)$s of the NPs and proteins. This suggests very little interaction between the NPs and the proteins, except perhaps in the case of PCL NP and Fg.

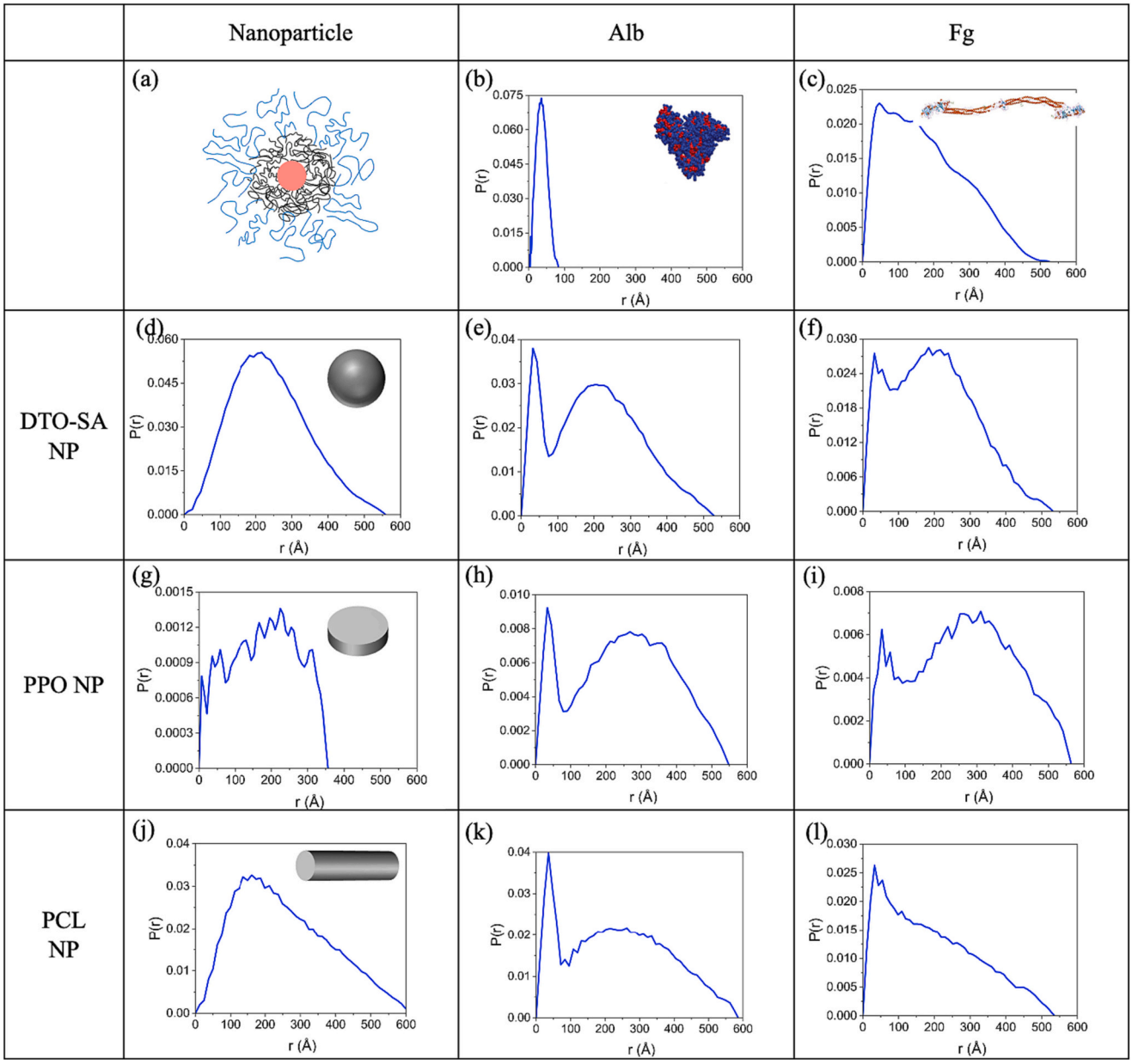

Fig. 5. SAXS data presented as pair distribution functions. Micelles are of different shapes; a sphere for DTO-SA NP, a disc for PPO NP, and a cylinder for PCL NP.

4. Discussion

The particles, i.e., adsorbates in our experiments, are immobilized by being adsorbed onto a hydrophobic surface; their binding to the substrate is sufficiently strong that they do not come off when rinsed with the buffer. An important finding in our work is that the interactions between two adsorbates near a surface depends on which one is adsorbed first. When a second adsorbate is allowed to be deposited after the first species has been adsorbed onto the substrate, we can envision one or more of the following six scenarios. The second adsorbate: (1) simply flows by without interacting with the adsorbed layer of the first species (e.g., NPs onto Fg); (2) is irreversibly adsorbed onto the layer of first adsorbate, which in some instances results in asymmetric behavior (e.g., PPO NP onto Alb and Fg onto DTO-SA NP); (3) is first adsorbed but then comes off upon rinsing via reversible adsorption (e.g., PCL NP onto Alb); (4) displaces the first adsorbate via complex formation via the Vroman effect (e.g., Alb displacing PCL NP); (5) is adsorbed and co-locates alongside the first adsorbate via surface remodeling (e.g., PCL NP onto Fg); (6) adheres to the pre-adsorbed adsorbate, but then carries this fragment away without staying adsorbed via ablation (e.g., Alb and Fg onto PPO NP). Note that although the Vroman effect was postulated to explain the behavior of plasma proteins, we are invoking it to explain the behavior of NPs as well [38]. There is no reason why nanoparticles, which are similar to proteins in size and, to some extent, surface charge distribution, should not exhibit the same behavior as proteins. All these types of behavior appeared to be present in our experiments as indicated in Fig. 3. We will attempt to explain these different modes of interactions in terms of the relative strengths of the pairwise interactions between the adsorbates and the hydrophobic substrate, the immobilized adsorbates and the molecules in solutions, and the adsorbates and the buffer medium.

The three NPs (~1000 kDa) used in this study have a similar hydrophilic PEG shell but have different hydrophobic core segments: DTO-SA that makes the core crystalline even in solution [17], PPO that makes the core amorphous, and PCL that is known to be crystalline when lyophilized [39], or dried [40]. Differences in the deployment of PEG

from the core of the NPs could affect the hydration layer, and thus influence protein adsorption. PCL is a diblock copolymer while PPO and DTO-SA are triblock; we do not expect this to significantly affect the adsorption characteristics and the interaction with proteins. The geometric or physical particle diameter of the NPs measured by small-angle x-ray scattering (SAXS) is similar at ~35 nm. The hydrodynamic diameter measured by DLS, which includes the hydrated shell, is much larger and also similar in all the three NPs, 40–50 nm [18]. Alb and Fg are the two plasma proteins used in this study. Alb (~66 kDa) can be modeled as a triangular prismatic solid of dimensions 3.15 × 8.4 × 8.4 × 8.4 nm [41], which is slightly smaller than the core of the NPs studied here (~10 nm). Fg (~ 342 kDa) can be modeled as a trinodular rectangular prism of size 1 × 6.5 × 46 nm [42], whose length is greater than the geometric diameter of the NPs (35 nm). The nodules at the ends are about the size of the core of the NPs. Differences in the size and the ratio of hydrophobic and hydrophilic groups on the surfaces of these two proteins contribute to the observed differences in adsorption behavior and their effect on the structure of the NPs. Because all the three NPs have a PEG outer layer, they all are hydrophilic. The two proteins used here are also hydrophilic. Thus, we do not expect large differences in surface energies (air-water contact angle) of the NP and the protein layers. Although the primary driving force is hydrophobic interactions, there are sufficient hydrophobic and hydrophilic residues on all faces in both proteins for them to be adsorbed onto hydrophilic, hydrophobic, and charged surfaces at several angles of approach [43].

QCMD data provides information about changes in the adsorbed mass and its viscoelastic properties. Interpretation of these data to identify the species that is adsorbed onto the substrate can be ambiguous. We are relying on XPS data to remove some of these ambiguities. However, XPS data are obtained in ultrahigh vacuum, while the QCMD experiments are carried out in aqueous media. This does not present a problem if only one species is being adsorbed and evaluated. The assumption in comparing the data from sequentially adsorbed species is that, although the adsorbates do deform upon drying and in vacuum, the second species to be adsorbed does not change places with the first; such changes would have occurred during the QCMD run.

4.1. Asymmetrical adsorption

If the adsorption to the substrate and other adsorbates were passive, then the resulting frequency shifts would be independent of the sequence in which the adsorption is carried out. An important finding from the QCMD data, and confirmed by XPS measurements, is that in all but two instances, (Alb paired with DTO-SA and Fg paired with PPO), the outcome depends on the sequence in which NPs and proteins they are adsorbed: (1) Fg binds to pre-adsorbed DTO-SA NP, but the opposite is not true. PCL NP also shows similar behavior; (2) PPO binds to pre-adsorbed Alb, but the opposite is not true. This asymmetric or sequence-dependent adsorption behavior is observed even between the NPs (Fig. S1). Note that the asymmetric adsorption behavior is observed only when the adsorbates bind to each other in some form. We attribute these characteristics to the immobilization and subsequent deformation and conformational changes of the adsorbates. The adsorption behavior is symmetric or bidirectional when there is no interaction between the adsorbates as in DTO-SA NP with Alb and PPO NP with Fg. The interaction between PCL NP and Alb follows Vroman behavior in that Alb with a stronger affinity to the substrate displaces PCL NP while PCL NP reversibly adsorbs onto pre-adsorbed Alb.

One of the questions that arises in the discussion of sequence-dependent adsorption is whether the species of adsorbates that arrive later interact with the layer of the first particle or, if the first adsorbate does not completely cover the surface, with the underlying hydrophobic polymer (E0000). Proteins are known to completely cover the surface, and it is unlikely that the larger NPs can find free spaces between the proteins to interact with the underlying substrate. Since there is a possibility that the NPs may not cover the complete surface [18], when the sequence is reversed such that protein comes after the deposition of the NPs, proteins could interact with the substrate Even if the NPs did cover the surface, proteins are small enough to fall between the spaces of the NPs to contact and adsorb to the underlying surface. Our data show this is not happening. Alb is known to adsorb onto E0000 [26], but in the data presented here, it does not adsorb onto the surface preabsorbed with DTO-SA and PPO NPs. Similarly, Fg adsorbs onto E0000 surface [44], but it does not adsorb onto the surface preabsorbed with PPO NP. Thus, there is no evidence that the proteins are interacting with underlying hydrophobic E0000 substrate, even if the coverage by NPs is incomplete. The interaction of the Fg or Alb with the pre-adsorbed NP layer appears to be different from that between the NPs and the pre-adsorbed Fg or Alb. Thus, the interactions between proteins and NPs when one of the species is adsorbed onto a substrate, or in practice to a tissue or a scaffold, cannot be predicted from their behavior in solution.

4.2. Conformational changes and deformation

In the three instances in which the later-arriving species irreversibly adsorbs onto the layer of adsorbates already on the substrate (d, e, and l in Figs. 2 and 3), the final thickness of the two adsorbed layers is close to being additive only when Fg is adsorbed to PCL NP. In the other two instances, when Fg is adsorbed onto DTO-SA NP and when PPO NP adsorbs onto Alb, the increase in thickness is less than the size of Fg and PPO NP, respectively. Since the deposition always reaches a plateau quickly, it is unlikely that there is partial adsorption of the second species. This suggests that the smaller total thickness is due to remodeling of the two deposited layers, a process in which the either or both the molecules undergo deformation. Large conformational changes of the adsorbates that occur as they are adsorbed onto substrates have been reported [11,13]. Proteins tend to spread upon adsorption [45,46]; their footprint depends on the adsorbed surfaces [11] and is higher on hydrophobic surfaces since the primary driving force for protein spreading is hydrophobic interactions between the protein and the substrate [43]. Deformation of the NPs upon adsorption has also been reported [18]. When NPs deform upon adsorption, the accompanying redistribution of the PEG chains and possible disassembly determines the hydrophobic-hydrophilic balance of the surface exposed to the incoming proteins. In some instances, it appears that the NP is fragmented and carried away by the incoming protein, resulting in a loss of mass; this is especially true in the case of PPO NP that binds to Alb and Fg.

Given the above discussed changes in the conformation upon adsorption, one would expect a different outcome when the sequence is reversed. Therefore, the asymmetry in the interactions reported in the previous section occurs because the NPs and proteins deform when they are adsorbed from solution either onto the pre-adsorbed protein and NP layers, respectively, or onto the hydrophobic E0000 surface.

4.3. Sequential adsorption mechanisms

It has been proposed that when multiple species are competing for adsorption onto a surface, the interaction between the species occurs in four stages: (1) an initial layer is formed from the first species to be adsorbed; (2) the second species to be deposited embeds itself into the initial layer forming a “transient complex”; (3) the second adsorbate, either protein or NP, binds to the first species and causes its orientation and possibly conformation to change, exposing the first layer to solution; (4) this triggers desorption of the first species, allowing the species with higher affinity to be adsorbed resulting in a surface that is enriched with the second species [47]. Thus, strong interaction or complex formation between the arriving and the adsorbed species is a prerequisite for resolving the paradox of how the second protein “knows” its affinity to the substrate is higher than that of the first protein that completely covers the substrate, as suggested by the Vroman effect, e.g., Alb displacing PCL NP [48,49]. The complex formation could also account for the proposed adsorption and co-location of the NP alongside Fg, or when

pre-adsorbed NP is fragmented by Fg.

4.4. Influence of NPs structure

Drug release from polymeric NPs is governed by their adsorption onto cell membranes and transmigration across cell walls. These steps are influenced by their interactions with proteins near the cells. The goal of this work was to understand these interactions, and hence the adsorption behavior of NPs and proteins onto substrates such as cell walls. The mechanics of such adsorption is a determined by pairwise interactions among the NPs, proteins and the substrate. Since the majority of NPs have a PEG shell, the expectation is that their interactions with proteins are similar, and that proteins in general would not adsorb onto the them [50]. The interactions of the NPs with proteins in the environment, which determine the composition of the protein corona around the NPs, are presumed to be determined by the chemical composition of the NPs' shells, for instance on the density of PEG chains [9]. But our data from three NPs with a similar PEG shell but different cores show that the core can modulate the NP-protein interactions. Similar observations have been made by studying core-crosslinked polymeric micelles [51]. These interactions near surfaces could be determined by the integrity of the NPs and how the PEG segments are deployed from their core segments. Most significantly, these differences in the interactions of the NPs seem to occur only with immobilized adsorbates; X-ray scattering data show little interaction between the NPs and the protein pairs when they are in solution (Fig. 4). This has implications on the NP assays because of the potential adsorption of the NPs onto glass and plastic surfaces during testing. More importantly, this indicates that solution data may not explain the adsorption measurements made on substrates that mimic the cell surfaces using techniques such as QCMD, surface plasmon resonance, ellipsometry, and x-ray or neutron reflectometry and may not be relevant to understanding the molecular interactions near substrates.

4.5. Implications for drug release

Poor delivery efficiency is one of the reasons why even after decades of research nanotechnology has not yet significantly improved drug delivery [52]. Only 0.7% (median) of the administered NP dose is found to be delivered to a solid tumor, resulting in a need for excess NP administration that causes higher costs, limited stability, and side effects due to the presence of the 99% of particles that do not deliver drug [14]. It has been suggested that size, shape, stiffness and surface functionalization, the '4S' parameters, play important roles in the transport of the NPs to tumor sites [16]. There have been efforts to control deformation by stabilizing the NPs, specifically by preventing premature disintegration of polymeric micelles, by crosslinking the core of micellar particles to improve their in vivo stability [51]. We show here that a knowledge of the stability of the micellar structure as it interacts with surfaces, cell membranes, and proteins is important in the design of NPs. An understanding of the mechanisms of deformation and possible subsequent dissociation of the NPs during their interaction with serum proteins and cell membranes is useful in developing methods to increase the delivery efficiency [16].

5. Conclusions

There could be as many as six modes of interactions between the adsorbed species and the later arrivals: no interaction, adsorption (reversible and irreversible), displacement, co-location, and ablation. Proteins and NPs deform upon adsorption onto substrates. As a result, the core of the NPs can modulate the deformation and thereby the interaction with proteins. Thus, solution studies may not reflect the interparticle interactions that occur near surfaces. Immobilization of adsorbates affects their interactions with other molecules that arrive later. Symmetrical interaction is not always observed, i.e., adsorption of one species onto another during sequential adsorption depends on the order in which these events occur. Displacement of pre-absorbed adsorbates, as per the Vroman effect generalized to include nanoparticles beyond the original application to plasma proteins, can be explained by changes in their conformation by adsorbates that arrive later and weaken the interactions between the first-adsorbed species and the substrate. Deformation and conformational changes of the adsorbates is also one of the reasons why the Vroman effect does not account for all the observed adsorption behaviors.

Author statement

Megan Maniar carried out most of the experimental work, prepared the figures, and wrote some of the sections the manuscript. Joachim Kohn provided the facilities to carry out this work and was involved in the discussion of the results. Sanjeeva Murthy conceptualized the work, carried out some of the experiments, prepared the figures, wrote the manuscript, and prepared the work for submission.

Declaration of Competing Interest

None.

Acknowledgments

The work was in part funded by the National Science Foundation (DMREF-2118860). This work was carried out using the resources at the New Jersey Center for Biomaterials. The authors acknowledge James Byrnes, beamline scientist at NSLS-II beamline 16-ID for Life Science X-ray Scattering (LiX), for his assistance with conducting experiments at Brookhaven National Laboratory. The LiX beamline is part of the Center for BioMolecular Structure (CBMS), which is primarily supported by the National Institutes of Health, National Institute of General Medical Sciences (NIGMS) through a P30 Grant (P30GM133893), and by the DOE Office of Biological and Environmental Research (KP1605010). LiX also received additional support from NIH Grant S10 OD012331. As part of NSLS-II, a national user facility at Brookhaven National Laboratory, work performed at the CBMS was supported in part by the U.S. Department of Energy, Office of Science, Office of Basic Energy Sciences Program under contract number DE-SC0012704.

Appendix A. Supplementary data

Supplementary data to this article can be found online at https://doi.org/10.1016/j.bpc.2023.107098.

References

[1] F. Gu, L. Zhang, B.A. Teply, N. Mann, A. Wang, A.F. Radovic-Moreno, R. Langer, O. C. Farokhzad, Precise engineering of targeted nanoparticles by using self-assembled biointegrated block copolymers, Proc. Natl. Acad. Sci. 105 (7) (2008) 2586–2591.
[2] V.P. Torchilin, Structure and design of polymeric surfactant-based drug delivery systems, J. Control. Release 73 (2) (2001) 137–172.
[3] K. Letchford, H. Burt, A review of the formation and classification of amphiphilic block copolymer nanoparticulate structures: micelles, nanospheres, nanocapsules and polymersomes, Eur. J. Pharm. Biopharm. 65 (3) (2007) 259–269.
[4] T. Dvir, B.P. Timko, D.S. Kohane, R. Langer, Nanotechnological strategies for engineering complex tissues, Nat. Nanotechnol. 6 (1) (2011) 13–22.
[5] X. Zheng, P. Zhang, Z. Fu, S. Meng, L. Dai, H. Yang, Applications of nanomaterials in tissue engineering, RSC Adv. 11 (31) (2021) 19041–19058.
[6] A. Hasan, M. Morshed, A. Memic, S. Hassan, T.J. Webster, H.E.-S. Marei, Nanoparticles in tissue engineering: applications, challenges and prospects, Int. J. Nanomedicine 13 (2018) 5637.
[7] S.R. Saptarshi, A. Duschl, A.L. Lopata, Interaction of nanoparticles with proteins: relation to bio-reactivity of the nanoparticle, Journal of Nanobiotechnology 11 (1) (2013) 1–12.
[8] S. Wilhelm, A.J. Tavares, Q. Dai, S. Ohta, J. Audet, H.F. Dvorak, W.C. Chan, Analysis of nanoparticle delivery to tumours, Nature Reviews Materials 1 (5) (2016) 1–12.

[9] K. Obst, G. Yealland, B. Balzus, E. Miceli, M. Dimde, C. Weise, M. Eravci, R. Bodmeier, R. Haag, M. Calderón, Protein corona formation on colloidal polymeric nanoparticles and polymeric nanogels: impact on cellular uptake, toxicity, immunogenicity, and drug release properties, Biomacromolecules 18 (6) (2017) 1762–1771.

[10] N. Bertrand, P. Grenier, M. Mahmoudi, E.M. Lima, E.A. Appel, F. Dormont, J.-M. Lim, R. Karnik, R. Langer, O.C. Farokhzad, Mechanistic understanding of in vivo protein corona formation on polymeric nanoparticles and impact on pharmacokinetics, Nat. Commun. 8 (1) (2017) 777.

[11] P. Satzer, F. Svec, G. Sekot, A. Jungbauer, Protein adsorption onto nanoparticles induces conformational changes: particle size dependency, kinetics, and mechanisms, Engineering in Life Sciences 16 (3) (2016) 238–246.

[12] D.H. Cho, J.-I. Hahm, Protein–polymer interaction characteristics unique to nanoscale interfaces: a perspective on recent insights, J. Phys. Chem. B 125 (23) (2021) 6040–6057.

[13] R.A. Latour, Biomaterials: protein-surface interactions, Encyclopedia of Biomaterials and Biomedical Engineering 1 (2005) 270–284.

[14] S. Wilhelm, A.J. Tavares, Q. Dai, S. Ohta, J. Audet, H.F. Dvorak, W.C. Chan, Analysis of nanoparticle delivery to tumours, Nature Reviews Materials 1 (5) (2016) 16014.

[15] T. Smart, H. Lomas, M. Massignani, M.V. Flores-Merino, L.R. Perez, G. Battaglia, Block copolymer nanostructures, Nano Today 3 (3–4) (2008) 38–46.

[16] H. Ye, Z. Shen, L. Yu, M. Wei, Y. Li, Manipulating nanoparticle transport within blood flow through external forces: an exemplar of mechanics in nanomedicine, Proceedings of the Royal Society A: Mathematical, Physical and Engineering Sciences 474 (2211) (2018) 20170845.

[17] N.S. Murthy, Z. Zhang, S. Borsadia, J. Kohn, Nanospheres with a smectic hydrophobic core and an amorphous PEG hydrophilic shell: structural changes and implications for drug delivery, Soft Matter 14 (8) (2018) 1327–1335.

[18] A. Patel, M.R. Lima, H.-Y. Cho, K.-B. Lee, N.S. Murthy, J. Kohn, Disassembly of nanospheres with a PEG shell upon adsorption onto PEGylated substrates, Langmuir 36 (1) (2019) 232–241.

[19] C. Yu, J. Kohn, Tyrosine–PEG-derived poly(ether carbonate)s as new biomaterials: part I: synthesis and evaluation, Biomaterials 20 (3) (1999) 253–264.

[20] N. Murthy, W. Wang, J. Kohn, Microphase separation in copolymers of hydrophilic PEG blocks and hydrophobic tyrosine-derived segments using simultaneous SAXS/WAXS/DSC, Polymer 51 (17) (2010) 3978–3988.

[21] J.C. Burrell, D. Bhatnagar, D.P. Brown, N.S. Murthy, J. Dutton, K.D. Browne, F. A. Laimo, Z.S. Ali, J.M. Rosen, H.M. Kaplan, Tyrosine-derived polycarbonate nerve guidance tubes elicit proregenerative extracellular matrix deposition when used to bridge segmental nerve defects in swine, J. Biomed. Mater. Res. A 109 (7) (2021) 1183–1195.

[22] C.M. Garrison, A. Singh-Varma, A.K. Pastino, J.A. Steele, J. Kohn, N.S. Murthy, J. E. Schwarzbauer, A multilayered scaffold for regeneration of smooth muscle and connective tissue layers, J. Biomed. Mater. Res. A 109 (5) (2021) 733–744.

[23] S. Saxena, W. Chang, A. Fakhrzadeh, N.S. Murthy, W. Zhang, J. Kohn, P.C. Yelick, Calcium phosphate enriched synthetic tyrosine-derived polycarbonate–dicalcium phosphate dihydrate polymer scaffolds for enhanced bone regeneration, Materialia 9 (2020), 100616.

[24] M.H.R. Magno, J. Kim, A. Srinivasan, S. McBride, D. Bolikal, A. Darr, J. O. Hollinger, J. Kohn, Synthesis, degradation and biocompatibility of tyrosine-derived polycarbonate scaffolds, J. Mater. Chem. 20 (40) (2010) 8885–8893.

[25] V. Tangpasuthadol, S.M. Pendharkar, R.C. Peterson, J. Kohn, Hydrolytic degradation of tyrosine-derived polycarbonates, a class of new biomaterials. Part II: 3-yr study of polymeric devices, Biomaterials 21 (23) (2000) 2379–2387.

[26] H.P. Felgueiras, S.D. Sommerfeld, N.S. Murthy, J. Kohn, V.R. Migonney, Poly (NaSS) functionalization modulates the conformation of fibronectin and collagen type I to enhance osteoblastic cell attachment onto Ti6Al4V, Langmuir 30 (31) (2014) 9477–9483.

[27] M.C. Dixon, Quartz crystal microbalance with dissipation monitoring: enabling real-time characterization of biological materials and their interactions, Journal of Biomolecular Techniques: JBT 19 (3) (2008) 151.

[28] F. Höök, B. Kasemo, T. Nylander, C. Fant, K. Sott, H. Elwing, Variations in coupled water, viscoelastic properties, and film thickness of a Mefp-1 protein film during adsorption and cross-linking: a quartz crystal microbalance with dissipation monitoring, ellipsometry, and surface plasmon resonance study, Anal. Chem. 73 (24) (2001) 5796–5804.

[29] F. Höök, M. Rudh, Quartz crystal microbalances (QCM) in biomacromolecular recognition, Review in BTi Molecular Biology Februrary (2005) 8–13.

[30] V.H. Perez-Luna, J. Kohn, D.J. Graham, B.D. Ratner, Poly (desaminotyrosyl-tyrosine carbonate ethyl ester) studied by XPS, Surface Science Spectra 9 (1) (2002) 6–11.

[31] J.B. Hopkins, R.E. Gillilan, S. Skou, BioXTAS RAW: improvements to a free open-source program for small-angle X-ray scattering data reduction and analysis, J. Appl. Crystallogr. 50 (5) (2017) 1545–1553.

[32] K. Reimhult, K. Petersson, A. Krozer, QCM-D analysis of the performance of blocking agents on gold and polystyrene surfaces, Langmuir 24 (16) (2008) 8695–8700.

[33] P. Sobolewski, N.S. Murthy, J. Kohn, M. El Fray, Adsorption of fibrinogen and fibronectin on elastomeric poly (butylene succinate) copolyesters, Langmuir 35 (26) (2019) 8850–8859.

[34] M.M. Ouberai, K. Xu, M.E. Welland, Effect of the interplay between protein and surface on the properties of adsorbed protein layers, Biomaterials 35 (24) (2014) 6157–6163.

[35] D.I. Svergun, M.H. Koch, Small-angle scattering studies of biological macromolecules in solution, Rep. Prog. Phys. 66 (10) (2003) 1735.

[36] M. Paar, V.H. Fengler, D.J. Rosenberg, A. Krebs, R.E. Stauber, K. Oettl, M. Hammel, Albumin in patients with liver disease shows an altered conformation, Communications Biology 4 (1) (2021) 1–9.

[37] A. Shpichka, P. Konarev, Y.M. Efremov, A. Kryukova, N. Aksenova, S. Kotova, A. Frolova, N. Kosheleva, O. Zhigalina, V. Yusupov, Digging deeper: structural background of PEGylated fibrin gels in cell migration and lumenogenesis, RSC Adv. 10 (8) (2020) 4190–4200.

[38] S. Darjani, J. Koplik, V. Pauchard, S. Banerjee, Adsorption kinetics and thermodynamic properties of a binary mixture of hard-core particles on a square lattice, J. Chem. Phys. 154 (7) (2021).

[39] Q. Zhang, E.E. Remsen, K.L. Wooley, Shell cross-linked nanoparticles containing hydrolytically degradable, crystalline core domains, J. Am. Chem. Soc. 122 (15) (2000) 3642–3651.

[40] Z.-X. Du, J.-T. Xu, Z.-Q. Fan, Micellar morphologies of poly (ε-caprolactone)-b-poly (ethylene oxide) block copolymers in water with a crystalline core, Macromolecules 40 (21) (2007) 7633–7637.

[41] M.L. Ferrer, R. Duchowicz, B. Carrasco, J.G. de la Torre, A.U. Acuna, The conformation of serum albumin in solution: a combined phosphorescence depolarization-hydrodynamic modeling study, Biophys. J. 80 (5) (2001) 2422–2430.

[42] I.S. Yermolenko, V.K. Lishko, T.P. Ugarova, S.N. Magonov, High-resolution visualization of fibrinogen molecules and fibrin fibers with atomic force microscopy, Biomacromolecules 12 (2) (2011) 370–379.

[43] C.F. Wertz, M.M. Santore, Effect of surface hydrophobicity on adsorption and relaxation kinetics of albumin and fibrinogen: single-species and competitive behavior, Langmuir 17 (10) (2001) 3006–3016.

[44] N. Weber, A. Pesnell, D. Bolikal, J. Zeltinger, J. Kohn, Viscoelastic properties of fibrinogen adsorbed to the surface of biomaterials used in blood-contacting medical devices, Langmuir 23 (6) (2007) 3298–3304.

[45] B. Snopok, E. Kostyukevich, Kinetic studies of protein–surface interactions: a two-stage model of surface-induced protein transitions in adsorbed biofilms, Anal. Biochem. 348 (2) (2006) 222–231.

[46] P. Roach, D. Farrar, C.C. Perry, Interpretation of protein adsorption: surface-induced conformational changes, J. Am. Chem. Soc. 127 (22) (2005) 8168–8173.

[47] S.L. Hirsh, D.R. McKenzie, N.J. Nosworthy, J.A. Denman, O.U. Sezerman, M. M. Bilek, The Vroman effect: competitive protein exchange with dynamic multilayer protein aggregates, Colloids Surf. B: Biointerfaces 103 (2013) 395–404.

[48] L. Vroman, A.L. Adams, Findings with the recording ellipsometer suggesting rapid exchange of specific plasma proteins at liquid/solid interfaces, Surf. Sci. 16 (1969) 438–446.

[49] L. Vroman, A.L. Adams, Identification of rapid changes at plasma–solid interfaces, J. Biomed. Mater. Res. 3 (1) (1969) 43–67.

[50] N.S. Murthy, W. Wang, S.D. Sommerfeld, D. Vaknin, J. Kohn, Temperature-activated PEG surface segregation controls the protein repellency of polymers, Langmuir 35 (2019) 9769–9776.

[51] M. Talelli, M. Barz, C.J. Rijcken, F. Kiessling, W.E. Hennink, T. Lammers, Core-crosslinked polymeric micelles: principles, preparation, biomedical applications and clinical translation, Nano Today 10 (1) (2015) 93–117.

[52] K. Park, Facing the truth about nanotechnology in drug delivery, ACS Nano 7 (9) (2013) 7442–7447.